第34卷 第1期 焊 接 学 报 Vol. 34 No. 1
2013年1月 TRANSACTIONS OF THE CHINA WELDING INSTITUTION January 2013

不同颗粒致密度 WC-10Co-4Cr 涂层的耐腐蚀性能

丁坤英， 程涛涛， 王志平
(中国民航大学 天津市民用航空器适航与维修重点实验室，天津 300300)


丁坤英

摘 要： 在300 M钢表面上，利用超音速火焰喷涂技术将两种不同颗粒致密度的WC-10Co-4Cr粉末制成涂层. 利用扫描电镜、X射线衍射仪、显微硬度计分析涂层的微观组织，通过极化试验和浸泡试验分析涂层的耐腐蚀性能. 结果表明，高颗粒致密度粉末制备的WC-10Co-4Cr涂层孔隙率为1.52%，是低颗粒致密度粉末制备涂层的1.95倍；在3.5% NaCl溶液中，高颗粒致密度粉末制备涂层的耐蚀性较差，腐蚀电流密度是低颗粒致密度粉末制备涂层的2.67倍. 低颗粒致密度粉末制备的涂层孔隙率低，对基体的保护性较好.

关键词： 颗粒致密度；超音速火焰喷涂；WC-10Co-4Cr涂层；孔隙率；耐腐蚀性能
中图分类号： TG178 **文献标识码：** A **文章编号：** 0253-360X(2013)01-0093-04

0 序 言

超音速火焰喷涂(high-velocity oxygen fuel，HVOF)技术是20世纪80年代研发出的热喷涂方法，具有适中的焰流温度(约3 000 ℃)和较高的焰流速度(最高达2 000 m/s)，制备的涂层具有高硬度和高耐磨性的特点，广泛应用于部件的表面耐磨防护[1]. 在航空制造领域，利用超音速火焰喷涂技术制备碳化钨耐磨涂层，替代起落架表面的电镀硬铬层，成为了该种涂层技术推广的研究热点[2-4]. 飞机起落架用材主要是300 M超高强钢，这种钢材在Cl^-环境中容易出现腐蚀问题. 因此起落架表面的碳化钨涂层在具有耐磨性能的同时还要具备耐蚀性能. 在碳化钨粉末中加入Cr元素，制备WCCoCr系防护涂层是解决该问题的方法之一. 国内外文献中对WCCoCr系涂层的研究主要集中在粉末的粒度分布、流动性、球形度等参数以及涂层的喷涂工艺上[5,6]. 在制粉过程中，由于方法的不同会造成碳化钨颗粒致密度的差异，关于碳化钨颗粒的致密度对涂层耐蚀性能的影响，目前国内外研究中鲜有报道. 因此文中主要利用超音速火焰喷涂技术在300 M钢基体上制备两种颗粒致密度的WC-10Co-4Cr涂层，比较两种涂层的微观组织结构及特征，重点研究两种涂层在Cl^-环境中的耐腐蚀性能.

收稿日期： 2011-11-18
基金项目： 工信部重大专项资助项目(2011zx04014-21)；中央高校基本科研费中国民航大学专项资助项目(ZXH2011D002)

1 试验方法

采用团聚烧结的方法将细小的碳化钨原料粉制备成直径为15~45 μm的球状颗粒，每个颗粒的密实程度表现为碳化钨喷涂粉末的颗粒致密度. 文中喷涂试验采用两种不同颗粒致密度的WC-10Co-4Cr粉末，其中各组元质量分数均为10% Co，4% Cr，其余为WC，粉末基本性能见表1.

表1 两种粉末基本性能指标
Table 1 Characteristics of two kinds of powder

粉末种类	型号	松装密度 ρ/(g·cm^{-3})	粒度范围 D/μm
高颗粒致密度粉末	A	4.72	15~45
低颗粒致密度粉末	B	3.95	15~45

基体材料为300 M超高强钢，喷涂设备为美国TAFA公司生产的JP5000型超音速火焰喷涂系统(HVOF)，涂层制备工艺参数见表2.

表2 涂层制备工艺参数
Table 2 HVOF coating spraying parameters

氧气流量 q_1/(m^3·h^{-1})	煤油流量 q_2/(cm^3·min^{-1})	喷涂距离 L/mm
1 900	23	380

利用德国LEO公司生产的1530VP型场发射扫描电子显微镜进行显微组织观察及成分分析，并利

用 Axioimager. A1m 图像分析系统对涂层显微组织进行分析; 利用 HVS-1000 型显微硬度仪测量试样的显微硬度,载荷为 2.94 N,加载时间为 20 s; 利用德国 Bruker-AXS 生产的 D8 Advance X 射线多晶衍射仪对涂层进行物相分析.

采用 Hasuncast3010 环氧树脂对极化试验及浸泡试验中的试样进行密封处理,保证每个试样只有 506.4 mm^2 的涂层面积暴漏出来. 利用德国 IM6ex 电化学工作站测定试样的电化学特性. 试样在 3.5% 的 NaCl 溶液中浸泡 90 min,然后进行电化学试验. 利用 Tafel plot 技术测定涂层试样的极化曲线,并利用 Tafel 外推法确定涂层试样的腐蚀电位 φ_c 及腐蚀电流密度 i_c,扫描范围为 -1 200 ~ +100 mV,扫描速度为 1 mV/s.

参考国家标准 GB/T 10834—2008 对试样进行浸泡试验. 试样在 3.5% 的 NaCl 溶液中进行周期为 192 h 的浸泡腐蚀试验,每隔 24 h 清洗腐蚀产物,称量失/增重量并记录,其中每组试样单位面积上失/增重量的值为 3 个试样的平均值.

2 粉末及涂层微观结构及特征

2.1 粉末及涂层形貌观察

图 1 为 A 型 WC-10Co-4Cr 粉末和 B 型 WC-10Co-4Cr 粉末扫描电镜观察形貌,从图 1 中可以看出,A 型粉末致密度高,具有较好的球形度; B 型粉末疏松多孔,球形度稍差,但颗粒的粒度均匀性较好.

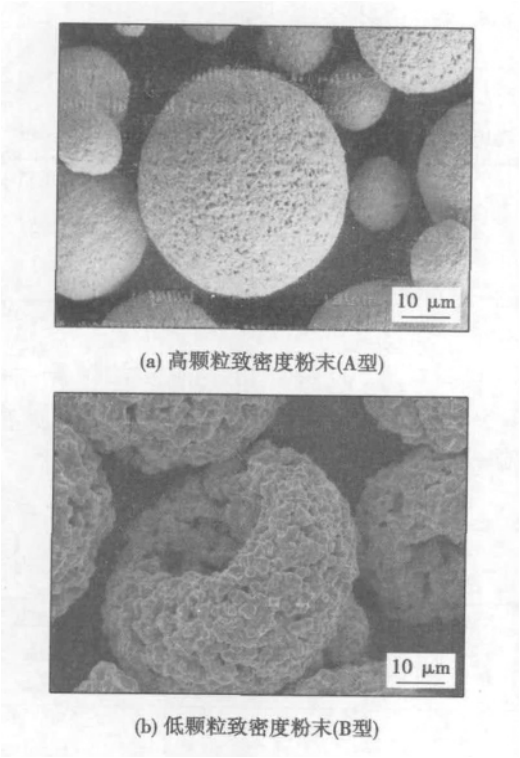

图 1 不同颗粒致密度 WC-10Co-4Cr 粉末形貌

Fig. 1 Two kinds of powder with different particle-density

对 A 型和 B 型粉末制备的超音速火焰喷涂 WC-10Co-4Cr 涂层进行显微观察(图 2),结果表明,两种涂层与基体材料都保持着良好的结合,涂层内部组织均匀,有少量弥散分布的孔洞. A 型粉末和 B 粉末制成涂层的孔隙率(每个试样测定选取 5 个视场,每组 3 个试样取平均值)分别为 1.52% 和 0.78%,显微硬度(每个试样取 10 个点,每组 3 个试样取平均值)分别为 1 218,1 167 HV.

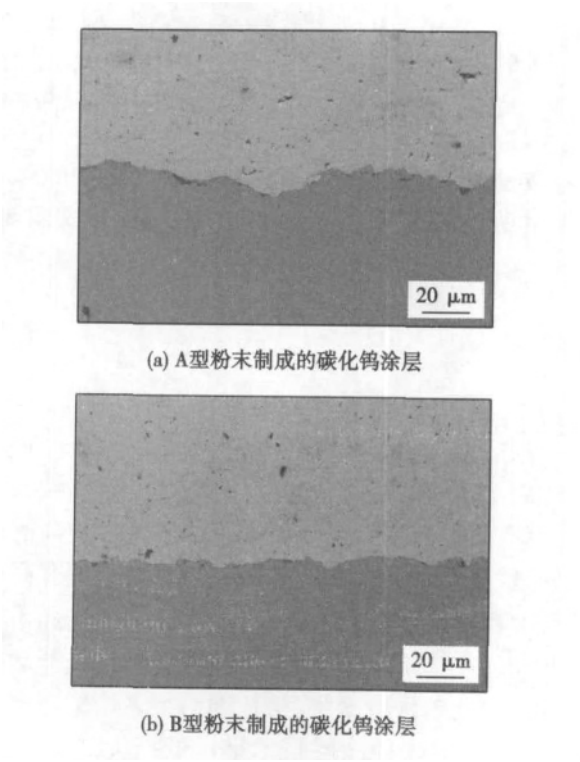

图 2 两种涂层的显微组织形貌

Fig. 2 Microstructures of two kinds of coatings

2.2 涂层物相检测

两种涂层的 XRD 检测结果如图 3 所示. 从图 3

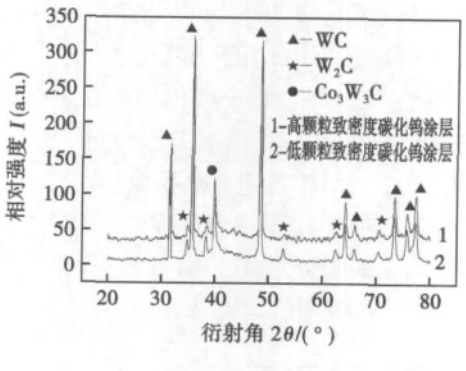

图 3 XRD 衍射图谱

Fig. 3 XRD patterns of two kinds of coatings

中可以看出,两种涂层的主要组成相为 WC,同时涂层中都出现了一定量的 W_2C 和 Co_3W_3C,说明两种粉末在制备涂层过程中均发生了不同程度的 WC 的氧化脱碳现象[7]. 经过计算,A 型粉末制备涂层的碳化钨分解率为 19.86%,B 型粉末制备涂层的碳化钨分解率为 14.45%,两种涂层的特性如表 3 所示.

表 3　两种涂层检测结果

Table 3　Characteristics of two kinds of coatings

试样	孔隙率 δ_1(%)	显微硬度 H_{HV}/GPa	WC 分解率 δ_2(%)
A 型粉末制备涂层	1.52	12.18	19.86
B 型粉末制备涂层	0.78	11.67	14.45

3　耐腐蚀试验结果及分析

3.1　极化试验

图 4 为以 300 M 钢为基体的两种颗粒致密度涂层试样在 3.5% NaCl 溶液中发生的极化现象. 利用 Tafel 外推法得到两种涂层试样的腐蚀电位 φ_c 及腐蚀电流密度 i_c,结果见表 4.

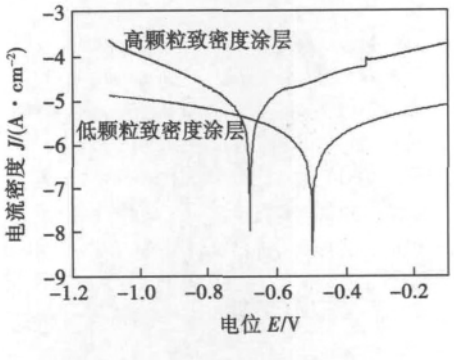

图 4　两种涂层试样的 Tafel 曲线

Fig. 4　Tafel plots of two kinds of coatings

表 4　两种涂层的电化学参数

Table 4　Electrochemistry parameters of two kinds of coatings

试样	腐蚀电位 φ_c/mV	腐蚀电流密度 i_c/(μA·cm^{-2})
A 型粉末制备涂层	-688	3.2
B 型粉末制备涂层	-506	1.2

从表 4 中可以看出,A 型粉末制备涂层的腐蚀电位明显低于 B 型粉末制备的涂层,其腐蚀电流密度为 B 型粉末制备涂层的 2.67 倍. 说明低颗粒致密度粉末制备的涂层的耐蚀性能优于高颗粒致密度粉末制备的涂层.

3.2　浸泡试验

图 5 为 A 型和 B 型粉末制备涂层在 3.5% 的 NaCl 溶液中进行周期为 192 h 的浸泡腐蚀试验后的称重结果. 从图 5 中可以看出浸泡腐蚀后两种试样都是增重的. A 型粉末制备的涂层 192 h 后增重为 50.5 mg,是 B 型粉末制备涂层的 1.83 倍. 并且随着浸泡时间的延长,A 型粉末制备涂层增重的速率明显高于 B 型粉末制备的涂层.

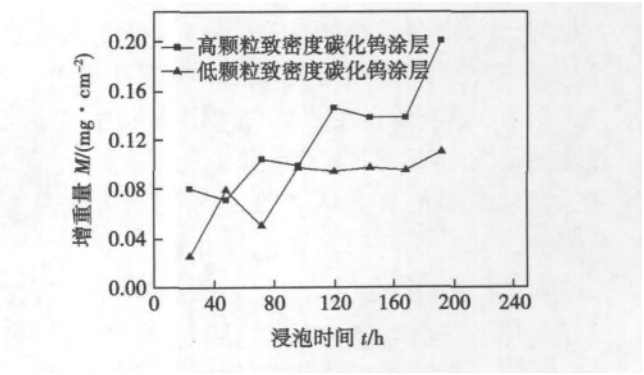

图 5　两种试样浸泡腐蚀后的重量变化对比

Fig. 5　Weight variants of two kinds of coatings after immersion

图 6 为两种试样浸泡腐蚀后界面处的显微组织形貌. 可以看出,A 型粉末制备的涂层的界面处基体腐蚀严重,已经形成了连续的腐蚀产物; 而 B 型

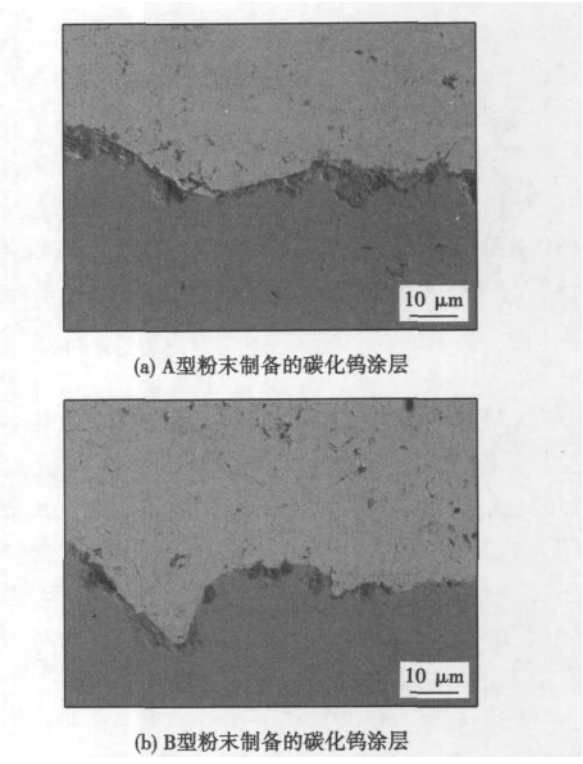

图 6　两种试样浸泡腐蚀后界面处的显微组织形貌

Fig. 6　Microstructures of intersection after immersion

粉末制备的涂层的界面处只是出现了局部区域的点蚀,并未形成连续的腐蚀,涂层与基体结合较好. 对两种试样浸泡腐蚀产物成分进行 EDS 分析,结果表明两种试样腐蚀产物主要为铁的氯化物及氧化物. 该结果说明浸泡腐蚀过程中界面处的腐蚀反应过程是溶液中的 Cl^- 以及溶解的 OH^- 与基体之间的反应.

3.3 综合分析

颗粒致密度对超音速火焰喷涂 WC-10Co-4Cr 涂层的孔隙率、显微硬度及 WC 分解率都有不同程度的影响,其中对涂层孔隙率的影响最为显著. A 型粉末由于颗粒致密度较高,在喷涂过程中铺展程度相对较低,因此更容易产生孔隙. 经过分析,A 型粉末制备涂层的孔隙率是 B 型粉末制备涂层的 1.95 倍. 300 M 钢为基体的碳化钨涂层试样在 3.5% NaCl 溶液中的腐蚀形式主要是腐蚀溶液穿过涂层的连通孔隙与 300 M 钢基体直接接触,Cl^- 对 300 M 钢产生孔蚀作用,直至腐蚀稳定[8-10]. 因为 A 型粉末制备的涂层孔隙率更高,所以在 3.5% NaCl 溶液环境中,腐蚀溶液更容易穿透 A 型粉末制备的涂层,对 300 M 钢基体造成腐蚀.

文中试验表明,颗粒的致密程度影响着喷涂过程中粉末的加热加速过程,并最终影响着涂层的结构特性和功能. 因此在喷涂粉末的选择过程中,除了考虑颗粒度、流动性、球形度以外,颗粒致密度也是应该重点考虑的因素.

4 结 论

(1) 在同一工艺条件下利用超音速火焰喷涂(HVOF)技术制备的两种颗粒致密度 WC-10Co-4Cr 涂层与基体材料都保持着良好的结合,界面处未见任何分离,内部组织均匀,仅有少量弥散分布的孔洞.

(2) 高颗粒致密度粉末制备的 WC-10Co-4Cr 涂层孔隙率、显微硬度及 WC 相的分解率分别为 1.52%,1 218 HV 和 19.86%,分别是低颗粒致密度粉末的 1.95 倍,1.04 倍和 1.37 倍. 颗粒致密度对超音速火焰喷涂 WC-10Co-4Cr 涂层的孔隙率、显微硬度及 WC 分解率都有不同程度的影响,而对涂层孔隙率的影响最为显著.

(3) 高颗粒致密度粉末制备的涂层由于孔隙率较高,腐蚀溶液容易渗透到基体与涂层界面,造成界面腐蚀. 而低颗粒致密度粉末制备的涂层对基体的保护性较好,具有较好的耐腐蚀性能.

参考文献:

[1] Voorwald H C, Souza R C. Evaluation of WC-17Co and WC-10Co-4Cr themal spray coatings by HVOF on the fatigue and corrosion strength of AISI 4340 steel [J]. Surface and Coatings Technology, 2005, 190(2/3): 155 - 164.

[2] 贾 鹏, 王志平, 李 娜, 等. 液体燃料 - 空气/氧气混合助燃超音速火焰喷涂枪的研制 [J]. 焊接学报, 2010, 31(6): 81 - 84.
Jia Peng, Wang Zhiping, Li Na, *et al*. Design of supersonic flame spraying gun with combustion-supporting of air-oxygen and liquid fuel [J]. Transactions of the China Welding Institution, 2010, 31(6): 81 - 84.

[3] Murthy J K, Venkataram B. Abrasive wear behaviours of WC-CoCr and Cr_3C_2-20(NiCr) deposited by HVOF and detonation spray processes [J]. Surface and Coatings Technology, 2006, 200(8): 2642 - 2652.

[4] Yang Q Q, Senda T, Ohmori A. Effect of carbide grain size on microstructure and sliding wear behavior of HVOF-sprayed WC-12% Co coating [J]. Wear, 2003, 254(1/2): 23 - 24.

[5] 徐连勇, 荆洪阳. 金属基陶瓷涂层/钢基体界面裂纹的应力强度因子 [J]. 焊接学报, 2008, 29(3): 84 - 88.
Xun Lianyong, Jing Hongyang. Stress intensity factor of interfacial crack between metal-base ceramic coating and steel [J]. Transactions of the China Welding Institution, 2008, 29(3): 84 - 88.

[6] Hasan M, Stokes J, Looney L, *et al*. Deposition and characterization of HVOF thermal sprayed functionally graded coating deposited onto a lightweight material [J]. Journal of Thermal Spray Technical, 2008, 18(1): 66 - 69.

[7] 郭面焕, 刘爱国, 赵敏海, 等. 等离子熔 - 喷 WC-17Co 涂层的组织结构 II [J]. 焊接学报, 2006, 27(6): 5 - 8.
Guo Mianhuan, Liu Aiguo, Zhao Minhai, *et al*. Microstructures of WC-17Co coating produced by plasma melt spraying II [J]. Transactions of the China Welding Institution, 2006, 27(6): 5 - 8.

[8] 赵卫民, 王 勇. NiCrBSi 超音速火焰喷涂层在水溶液中的腐蚀行为 [J]. 中国腐蚀与防护学报, 2004, 24(1): 37 - 40.
Zhao Weimin, Wang Yong. Study on the corrosion behavior of HVOF NiCrBSi coatings [J]. Journal of Chinese Society for Corrosion and Protection, 2004, 24(1): 37 - 40.

[9] 马 光, 于艳爽. 活性燃烧高速火焰喷涂 WC-CoCr 涂层的微观组织及性能 [J]. 金属热处理, 2008, 33(2): 36 - 40.
Ma Guang, Yu Yanshuang. Microstructure and properties of AC-HVAF sprayed WC-CoCr coating [J]. Heat Treatment of Metels, 2008, 33(2): 36 - 40.

[10] Gobinda C S, Tahir I K. The corrosion and wear performance of microcrystalline WC-10Co-4Cr and near-nanocrystalline WC-17Co high velocity oxy-fuel sprayed coatings on steel substrate [J]. Metallurgical and Materials Transactions A, 2010, 41(11): 3000 - 3009.

作者简介: 丁坤英,男,1981 年出生,博士研究生,讲师. 主要研究方向为表面加工工程. 发表论文 10 余篇. Email: dingkunying@126.com

minimal effect on BSCF. The influence rules of joint geometric parameters on BSCF at the weld toe show that the cover pass width has some influence on BSCF, the reinforcement and the weld toe radius both have little influence on BSCF. BLCC of under-matched butt joint can be improved by choosing appropriate joint geometric parameters.

Key words: high strength steel; under-matched butt joint; joint geometric parameters; bending stress concentration factor

Effect of sulphur on silver filler metal and brazing properties ZHANG Guanxing[1], LONG Weimin[1], BAO Li[1], SUI Fangfei[2] (1. State Key Laboratory of Advanced Brazing Filler Metals, Zhengzhou Research Institute of Mechanical Engineering, Zhengzhou 450001, China; 2. School of Materials Science & Engineering, Zhengzhou University, Zhengzhou 450001, China). pp 77 - 80

Abstract: The properties of sulphurized silver based solder were studied by optical microscope, scanning electron microscopy and other analytical tools. The experimental results indicate that the tensile strength of sulphurized filler metal decreased significantly, and then to a certain extent until not varied. The difference of wettability was obvious at different sulphurizing time. The wetting area was reduced by nearly half at the sulphurizing time of 30 min, but the wetting area of brazing filler metal would change little if the sulphurizing time further lasted. Relative dense sulphurized layer was formed on the surface of brazing filler metal and its thickness was about 10 μm. The distribution of Zn and Cu in the sulphurizing layer and the internal brazing filler metal is relatively uniform, while the Ag element is distributed periodically. Sulfur existed in the form of Ag_2S, Cu_2S, CuS and ZnS in the brazing filler metal. The melting points of Ag_2S, Cu_2S, CuS and ZnS were relatively high, and their existence would affect the welding properties severely.

Key words: sulfurizing; wettability; tensile strength; sulfide

Effects of laser micro-joining on microstructure and corrosion resistance of glass-ceramic coatings CHEN Pinghu[1], QIU Changjun[1], CHEN Yong[2], LONG Chongsheng[3] (1. School of Mechanical Engineering, Nanhua University, Hengyang 421001, China; 2. College of Materials Science and Engineering, Chongqing University, Chongqing 400030, China; 3. Nuclear Power Institute of China, Chengdu 610041, China). pp 81 - 84

Abstract: The high-temperature sintering and ball milling were adopted to prepare SiO_2 glass and Cr_2O_3 ceramic composite powder. The glass-ceramic coating was prepared by using the high-velocity flame spraying on the surface of 45 steel. And laser micro-joining techniques were used as secondary treatment in order to improve its properties. Effect of laser micro-joining on microstructure and properties of glass-ceramic coatings were investigated. The results showed that the laser micro-joining method being taken as the secondary treatment, the compactness of the coating is improved and the coatings becomes more uniform, and the micropores and crack in the glass-ceramic coating are reduced; the bonding strength of the interface, hydrophobic properties and corrosion resistance of the coatings are enhanced obviously. Consequently, the comprehensive performance of the glass-ceramic coatings is dramatically enhanced when laser micro-joining is adopted as the secondary treatment.

Key words: glass-ceramic coatings; laser micro-joining; hydrophobic properties; corrosion resistance; bonding strength

Effect of alloy elements on microstructure and phase structure of laser cladding Fe-based coatings NIE Binying[1], YAO Chengwu[2] (1. Chemical and Biological Engineering College, Yichun University, Yichun 336000, China; 2. Shanghai Key Laboratory of Materials Laser Processing and Modification, Shanghai Jiaotong University, Shanghai 200240, China). pp 85 - 88

Abstract: Four types of Fe-based alloys were fabricated on 45 carbon steel substrate by CO_2 laser surface cladding, and the effect of alloy elements on the microstructure and carbides of the coatings was investigated. With the increasing of the elements V, Nb, Ti, CeO in turn, the structure of the coating was transformed from the columnar crystal to columnar dendrites, and finally to the dendrite. With the simultaneous addition of the two elements V, Nb in the coating, the long strip carbides in the interdendritic region split into blocky carbides. At last, the carbides in the interdendritic region of the coating can be refined and spheroidized by adding elements V, Nb, Ti, CeO. The tensile test results showed that the tensile strength and elongation rate of the coating with dendritic structure and spheroidized carbides in the interdendritic region increased greatly, and the coating had high strength-toughness properties.

Key words: laser cladding; Fe-based alloy; alloy elements; microstructure morphology; carbides

Fracture characteristic of fiber laser-arc hybrid welded joints of 400 MPa grade ductile cast iron ZHENG Shiqing[1], LIU Zhu[1], SHAN Jiguo[1,2], WEN Peng[1,2] (1. Department of Mechanical Engineering, Tsinghua University, Beijing 100084, China; 2. Key Laboratory for Advanced Materials Processing Technology, Ministry of Education, Tsinghua University, Beijing 100084, China). pp 89 - 92

Abstract: Laser-MIG arc hybrid welding was used to weld 400 MPa grade ductile cast iron, which is used on key parts of wind power. The thickness of base metal is 5 mm, and 308L stainless steel wire was used as filler wire. The welds with good appearance and full penetration were obtained, and then the influence of welding conditions on tensile properties and fracture characteristic of joints was studied. The results show that the joint at low arc heat input has low tensile properties, fracture expands along the fusion line and it is brittle; the joint at high arc heat input has high tensile properties, fracture expands along base metal, which is brittle on the top of the joint and flexible at the bottom of the joint. The difference of joints fracture characteristic is caused by different quantities of ledebutire at the bottom of fusion zone and partial melting zone (PMZ) of the joints. Based on previous research results, a joint with the tensile strength of 346.4 MPa, the elongation of 5.4% was obtained and its fracture expands along base metal.

Key words: fiber laser-MIG arc hybrid welding; ductile cast iron; fracture characteristic; arc heat input

Corrosion resistance of different particle-density WC-10Co-4Cr coatings DING Kunying, CHENG Taotao, WANG

Zhiping (Tianjin Key Laboratory for Civil Aircraft Airworthiness and Maintenance, Civil Aviation University of China, Tianjin 300300, China). pp 93 – 96

Abstract: Two kinds of WC-10Co-4Cr coatings with different particle-density were deposited on 300M steel by high-velocity oxygen fuel (HVOF) technology. The microstructure and properties of WC-10Co-4Cr coatings were assessed by scanning electron microscope (SEM), X-ray diffraction (XRD) and micro-hardness tester. The corrosion resistance of the two kinds of coatings in a 3.5% NaCl solution was investigated by polarization test and immersion test. The results indicated that the porosity ratio of high particle-density coating was 1.52%, which was 1.95 times as big as that of low particle-density coating. In the NaCl solution, the value of passivation current density of high particle-density coating was 3.2 μA/cm^2, which was 2.67 times as big as that of low particle-density coating. Therefore, low particle-density coating exhibited superior corrosion resistance than high particle-density coating due to its less porosity.

Key words: particle-density; high-velocity oxygen fuel; WC-10Co-4Cr coating; porosity ratio; corrosion resistance

Improved ICP registration in 3-D model reconstruction

TU Zhiqiang[1], ZHANG Ke[1], YANG Chenglong[2], ZHU Xiaopeng[1], HUANG Jie[1] (1. Shanghai Key Laboratory of Laser Manufacturing & Material Modification, Shanghai Jiaotong University, Shanghai 200240, China; 2. Dalian Shipbuilding Industry Group Co., Ltd., Dalian 116005, China). pp 97 – 100

Abstract: One algorithm to automatically register point cloud data in 3-D model reconstruction was proposed. In the algorithm, the initial registration transformations were firstly calculated according to the curvature and normal vector of the point cloud. Then the best initial registration transformation was selected by geometric hashing method and the initial registration was completed by this transformation. Next, the ICP (iterative closest point) algorithm was improved by redefining the nearest point: For one measured point of ***A***, the nearest three points in ***B*** point cloud were firstly found; the triangle was formed by this three points and the foot point of this triangle was taken as nearest point of measured point. Then the improved ICP algorithm was used for accurate secondary registration. Finally, this algorithm was used to register the point data in previous model. And the results show this algorithm has the better performance in registration accuracy.

Key words: point cloud registration; iterative closest point; 3D reconstruction; laser remanufacturing

Analysis on microstructure and mechanism of extrusion-resistance welding for Cu-Al casing pipe

ZHAO Yue[1], ZUO Tiejun[2], LING Yong[3], ZUO Ke[1], WANG Xin[1] (1. School of Materials Science and Engineering, Ocean University of China, Qingdao 266100, China; 2. Qingdao Haiqing Machinery Plant, Qingdao 266021, China; 3. Belgian National Industry Research Institute, Zwijnaarde 9359052, Belgium). pp 101 – 104

Abstract: The extrusion-resistance welding was developed to join Cu-Al casing pipe. The welded joints have characteristics of high cleanliness and high peel strength, without assistants and filling material. This technology has been widely used in refrigeration industry for the welding of various sized pipes. The microstructure of the Cu-Al joint was analyzed by SEM and TEM. The results show that Cu-Al joints made by extrusion-resistance welding are mainly composed of solid solution and intermetallic compounds (IMCs) (α, Al_2Cu and Al_4Cu_9). The high temperature generated by the resistance heat and pressure leads to the formation of new phase. The pressure exerted by the mandril extrudes the brittle composition, and enlarges the contact area, which makes the columnar grain easily formed.

Key words: Cu-Al pipe; extrusion-resistance welding; refrigerant pipeline; microstructure

Influence of laser offset on microstructure and mechanical properties of Ti/Al dissimilar joint by laser welding

SONG Zhihua[1], WU Aiping[1], YAO Wei[2], ZOU Guisheng[1], REN Jialie[1], WANG Yongyang[2] (1. Key Laboratory for Advanced Materials Processing Technology of the Ministry of Education, Tsinghua University, Beijing 100084, China; 2. Beijing Hangxing Technology Development Co., Ltd., Beijing 100013, China). pp 105 – 108

Abstract: Laser welding of TA15 and 5A06 alloys with 3 mm in thickness was conducted by focusing laser beam on titanium side, and the aluminum was melted through the heat conduction from titanium side. The effect of laser offset distance on microstructure and mechanical properties of the dissimilar butt joint was investigated. When the laser offset is 0.1-0.4 mm, fusion welded joint is formed. When the laser offset is 0.5 mm, fusion welded joint is formed on the upper side of the joint accompanying with Ti-Al intermetallic compounds. Welded-brazed joint is formed on the middle and bottom side of the joint accompanying with continuous Ti-Al intermetallic compounds layer with 1 μm thickness. The tensile strength of joints firstly increased and then decreased with the laser offset increasing. The highest average tensile strength of the joint reaches 181 MPa when the laser offset distance is 0.5 mm. The joints partly fracture in Ti-Al intermetallic compounds at the interface, and partly fracture at the fusion zone of aluminum alloy.

Key words: titanium alloy; aluminum alloy; laser welding; microstructure; mechanical property

Effects of annealing and hot-rolling on properties and microstructure of explosion-welded composite steel plate

LIAO Dongbo[1], ZHA Wusheng[1], LI Wei[1,2] (1. College of Materials Science and Engineering, Xihua University, Chengdu 610039, China; 2. Yibin North Xin'an Composite Materials Co., Ltd., Yibin 644221, China). pp 109 – 112

Abstract: The mechanical properties and microstructure of as-welded, as-annealed and as-rolled stainless steel-carbon steel composite plates produced by explosive welding were investigated by SEM and mechanical tests. The element diffusion of transition layer formed in explosive welding was measured by EDS linear scanning. The results show that both the annealing and the hot-rolling can reduce the tensile strength and yield strength of the composite plates, but improve the ductility and toughness of the composite plates. The microstructure of the transition layer of as-welded, as-annealed and as-rolled composite plates are different. The wavy interface of the as-annealed composite plate is similar to that of as-welded composite plates. The diffusion layer with thickness of only about 5 μm is formed. For as-rolled composite plate, the wavy interface disappears and the diffusion layer enlarges to about 20 μm in width.

Key words: explosion-welded composite plate; hot rolling; annealing; mechanical properties; microstructure